Experimental Measurement of Speeds of Sound in Dense Supercritical Carbon Monoxide and Development of a High-Pressure, High-Temperature Equation of State

ARTICLE *in* THE JOURNAL OF PHYSICAL CHEMISTRY B · APRIL 2013

Impact Factor: 3.3 · DOI: 10.1021/jp401510m · Source: PubMed

6 AUTHORS, INCLUDING:

Joseph M Zaug

Lawrence Livermore National Laboratory

121 PUBLICATIONS **1,187** CITATIONS

SEE PROFILE

Michael R. Armstrong

Lawrence Livermore National Laboratory

71 PUBLICATIONS **664** CITATIONS

SEE PROFILE

THE JOURNAL OF PHYSICAL CHEMISTRY B

Article

pubs.acs.org/JPCB

Experimental Measurement of Speeds of Sound in Dense Supercritical Carbon Monoxide and Development of a High-Pressure, High-Temperature Equation of State

Joseph M. Zaug,* Jeffrey A. Carter, Sorin Bastea, Michael R. Armstrong, Jonathan C. Crowhurst, and Laurence E. Fried

Chemical Science Directorate, Lawrence Livermore National Laboratory, Livermore, California, 94550, United States

ABSTRACT: We report the adiabatic sound speeds for supercritical fluid carbon monoxide along two isotherms, from 0.17 to 2.13 GPa at 297 K and from 0.31 to 3.2 GPa at 600 K. The carbon monoxide was confined in a resistively heated diamond-anvil cell, and the sound speed measurements were conducted in situ using a recently reported variant of the photoacoustic light scattering effect. The measured sound speeds were then used to parametrize a single site dipolar exponential-6 intermolecular potential for carbon monoxide. PρT thermodynamic states, sound speeds, and shock Hugoniots were calculated using the newly parametrized intermolecular potential and compared to previously reported experimental results. Additionally, we generated an analytical equation of state for carbon monoxide by fitting to a grid of calculated PρT states over a range of 0.1−10 GPa and 150−2000 K. A 2% mean variation was found between computed high-pressure solid-phase densities and measured data—a surprising result for a spherical interaction potential. We further computed a rotationally dependent fluid to β-solid phase boundary; results signal the relative magnitude of short-range rotational disorder under conditions that span existing phase boundary measurements.

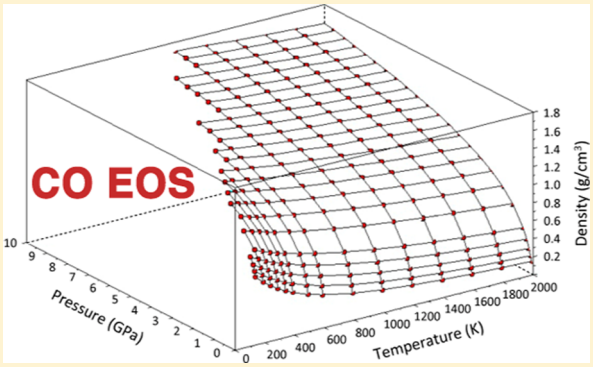

I. INTRODUCTION

The fluid properties of highly compressed carbon monoxide (CO) are of primary interest to detonation and planetary sciences, where extreme temperatures and pressures are commonplace. Carbon monoxide is an important equilibrium species in carbon-, oxygen-, and hydrogen-dominated metamorphic and igneous fluids with in the earth.[1,2] Research toward understanding the geochemical carbon cycle has observed CO as a byproduct—during the formation of a high-pressure polymorph of carbonate—in a previously unknown reaction forming a quenchable Mg−Fe carbon containing material.[3] As this avenue of exploration continues, more observations of CO will certainly appear. Carbon monoxide is also an oxidation intermediate or a product of an incomplete combustion of carbon-based materials and is thus important for the detonation of carbon-rich energetic materials.[4] Understanding the equilibrium of carbon oxidation under detonation conditions is necessary to improve the accuracy of thermochemical modeling and performance predictions.

The nature of dense hot environments precludes the direct measurement of equilibrium concentrations. Therefore, a statistical mechanics approach is taken to calculate thermodynamic equilibria or other thermodynamic properties of interest using equations of state (EOSs) as input.[1,5] Pressure dependent speed of sound measurements are a sensitive probe of the intermolecular potential energy landscape, which is subsequently used to obtain necessary EOSs.[6]

Previous thermodynamic measurements of CO fluids have been reported for pressures up to ∼1 GPa for static compression,[7−13] and up to ∼70 GPa using dynamic or shock compression.[14,15] Guided by these published data, various EOS models with different forms have been parametrized and can be found in the literature for fluid carbon monoxide.[8,10,11,16−20] This manuscript describes new, higher-pressure sound-speed measurements for CO along the 297 K isotherm from 0.17 to 2.13 GPa, and along the 600 K isotherm from 0.31 to 3.2 GPa. These measurements were subsequently used to further constrain the dipolar exponential-6 intermolecular potential[21] of CO, which is defined by the intermolecular interaction potential:

$$V_{ij}(\mathbf{r}_{ij}) = \varepsilon\left[Ae^{-a(r_{ij}/r_0)} - B\left(\frac{r_0}{r_{ij}}\right)^6\right] + \frac{r_{ij}^2\mu_i\cdot\mu_j - 3(\mu_i\cdot\mathbf{r}_{ij})(\mu_i\cdot\mathbf{r}_{ij})}{r_{ij}^5}$$

Received: February 11, 2013
Revised: April 12, 2013
Published: April 15, 2013

   dx.doi.org/10.1021/jp401510m | J. Phys. Chem. B 2013, 117, 5675−5682

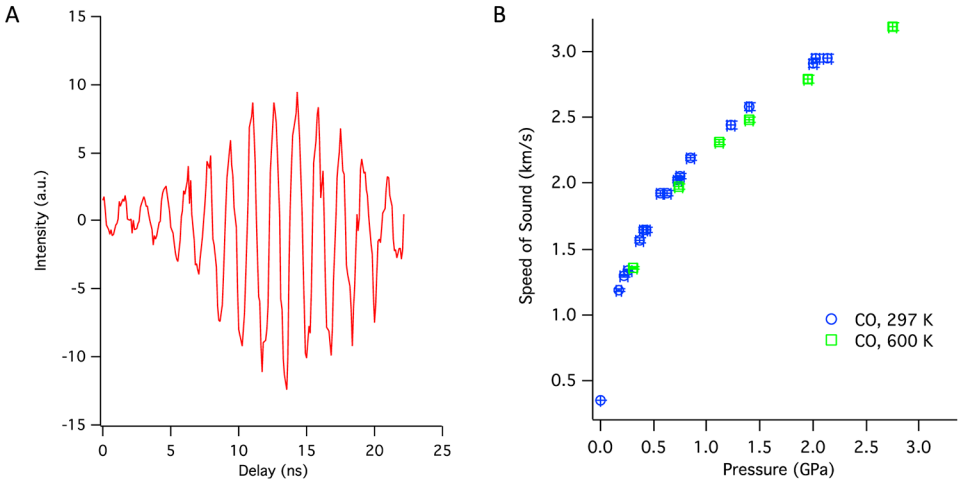

Figure 1. (A) Representative interference trace from PALS experiment for CO at 0.65 GPa and 297 K. Note the somewhat subtle phase discontinuity at ~17 ns, which occurs as the broadband pulse traverses the ion-etched line in the diamond. (B) Pressure-dependent sound speed data for carbon monoxide at 297 K (blue circles) and 600 K (green squares).

In this equation, $\mathbf{r}_{ij}$ is the displacement vector between molecules i and j, while r_{ij} is the intermolecular distance. ϵ is the well depth of the exponential-6 potential, r_0 is the distance between molecules, and α controls the steepness of the potential well. μ is the molecular dipole moment vector. $A = 6\exp(\alpha)/(\alpha - 6)$ and $B = \alpha/(\alpha - 6)$.

The sound speeds were measured using a recently developed variant of photoacoustic light scattering (PALS), which has technical advantages when compared to the traditional laser-based techniques for measuring sound speeds under high pressure and temperature conditions.[22] The PALS technique utilizes a pair of metal strips oriented perpendicular to the acoustic wave vector. One strip serves as a photoacoustic transducer, i.e., pump laser energy is efficiently deposited directly into the metal strip, which subsequently expands and launches a broadband, acoustic pulse that propagates through the fluid of interest at the material-dictated sound speed. This eliminates the usual requirement of direct coupling between the material of interest and the laser pulse for transient grating experiments. A time-delayed probe pulse then scatters from both the acoustic wave and a second, stationary parallel strip (not necessarily a metal strip; see below). Light scattered from the moving acoustic wave is Doppler shifted to a different frequency, and light scattered from the stationary strip is unshifted, and acts as a local oscillator. The signal is the intensity of the sum of the fields scattered into a specific wavevector. This intensity beats as the phase between the two fields varies as a function of the pump−probe delay. In particular, as the pump−probe delay increases, the distance between the scattering sources decreases, and the relative phase of the scattering sources changes accordingly. The resultant delay-dependent signal is a sinusoidal intensity oscillation, where the frequency depends on the sound speed of the fluid, the probe wavelength, and the difference between the incident and scattered wavevectors.[22] Carbon monoxide has negligible absorption strength at a pump wavelength of 1.064 μm and experiences pressure-induced chemical instability that is exacerbated above 3.2 GPa with visible and UV laser irradiation.[23] These factors make PALS an advantageous method for sound speed measurements within materials exhibiting similar properties as fluid CO.

II. EXPERIMENTAL SECTION

Carbon monoxide (99.998%) was obtained from Matheson and was loaded into a diamond-anvil cell (DAC) as a cryogenic fluid. A Lawrence Livermore National Laboratory (LLNL)-designed symmetric type DAC was constructed from Nimonic 80A superalloy. The sample chamber consists of two counter opposed low fluorescence type-I diamonds with 400-μm diameter culets, and an iridium gasket for sample confinement. The 4 μm × 159 μm platinum strip, serving as the photoacoustic transducer, was deposited on the diamond culet using a previously described procedure.[22] For this study, a 60-nm deep channel was milled into the diamond culet using a reactive ion beam, which functioned as the scattering source to generate the local oscillator. The 0.6 μm × 159 μm channel was oriented parallel to the platinum strip with a separation distance of 30 μm.

The Sm^{2+} fluorescence from an $Sm:SrB_4O_7$ crystal confined within the DAC chamber served as an optical manometer with a 0.03-GPa precision.[24] The $Sm:SrB_4O_7$ fluorescence, excited by the 488-nm line (<1 mW) of a continuous-wave argon-ion laser (Spectra-Physics), was dispersed and detected with an integrated spectrograph-CCD setup (LabRAM, Horiba) with the necessary resolution to obtain the 0.03-GPa precision. A pneumatic drive system (Betsa) was employed to change the sample pressure without altering the PALS optical alignment. Pressure was determined before and after each acoustic measurement. Time-dependent drifts in pressure—typically <0.2 GPa—were used to determine a corresponding pressure for each acoustic measurement. The temperature was regulated to within 0.1 K by a proportional-integral-derivative PID-controlled platinum-wire heater, which surrounds the sample chamber. The DAC sample temperature was measured using a type-k thermocouple secured by Resbond 940LE ceramic cement to within 1−2 mm of a diamond culet.

The optical layout employed for these sound speed measurements has been previously discussed.[22] The 100-ps duration output pulses of a regenerative amplified Nd:YAG system (Jaguar, Time-Bandwidth Products) with a repetition rate of 3.748 kHz are split into pump and probe pulses. The pump pulses travel through a chopper wheel reducing the repetition rate to 1.874 kHz and then are focused down to a

dx.doi.org/10.1021/jp401510m | J. Phys. Chem. B 2013, 117, 5675−5682

spot size ~20 μm and attenuated such that the peak irradiance is less than 0.03 GW/cm^2 at the photoacoustic transducer. The probe pulses are frequency doubled to 532 nm, travel through a computer-controlled time-of-flight optical delay, and are then focused to ~20-μm spot size in the sample plane. The interference of the two scattering sources is focused on a photomultiplier tube (Pacific Instruments with a 10× in-line fast signal amplifier) sampling a solid angle of 5×10^{-3} msr and is collected by a boxcar integrator (Stanford Research Systems). Each data point in the time-domain trace is an average of 800 laser shots and obtained at 100-ps pump−probe delay intervals. Under the conditions described above, a typical PALS measurement takes between 60 and 90 s to complete. For absolute determination of the sound speed of carbon monoxide, the collection wavevector was experimentally determined by measuring and comparing to the accepted sound speed of water.[24]

III. RESULTS AND DISCUSSION

Interferometric PALS data were collected at various pressures between 0.17 and 3.19 GPa along the 297 and 600 K isotherms. Figure 1A shows a representative raw data set, which is characterized by a carrier frequency υ and an amplitude-modulating envelope shape. The carrier frequency is related to the sound speed c of the material through the relation $c = \upsilon/k_{eff}$, where k_{eff} is the experimentally determined effective wavevector of the collected signal,[22] and is a function of the collection geometry and the probe wavelength. The raw data is Fourier transformed to obtain the carrier frequency, and the reported error in sound speed is propagated from the uncertainty in the peak frequency. The measured pressure-dependent sound speeds for carbon monoxide are displayed in Figure 1B and tabulated in Table 1. Despite the 2x increase in absolute temperature, the sound speeds along the two isotherms are quite similar, differing at most by ~5% at the same pressure. Temperature affects the sound speeds primarily through thermal expansion, which, for a fluid compressed to several GPa is minimal.[25]

Table 1. Speeds of Sound for Carbon Monoxide along the Noted Isotherms[a]

297 K		600 K	
P (GPa)	c (km s^{-1})	P (GPa)	c (km s^{-1})
0.17	1.186 (0.013)	0.31	1.356 (0.014)
0.22	1.293 (0.014)	0.74	1.970 (0.020)
0.26	1.333 (0.014)	1.12	2.312 (0.023)
0.37	1.564 (0.017)	1.40	2.485 (0.025)
0.40	1.646 (0.017)	1.95	2.794 (0.028)
0.43	1.650 (0.017)	2.75	3.193 (0.032)
0.57	1.920 (0.020)	3.02	3.311 (0.033)
0.63	1.920 (0.020)	3.02	3.300 (0.033)
0.73	2.028 (0.022)		
0.75	2.053 (0.022)		
0.85	2.192 (0.023)		
1.23	2.443 (0.026)		
1.40	2.583 (0.028)		
2.00	2.908 (0.029)		
2.02	2.949 (0.031)		
2.13	2.950 (0.030)		

[a]Uncertainties in sound speeds are shown in parentheses. The nominal uncertainty in determined pressure is 0.03 GPa.

The physical properties, including sound speeds, of CO have historically been compared to molecular nitrogen (N_2) due to the isoelectronic relationship.[26−28] While chemically, these two molecular species are strikingly different, the physical properties are remarkably similar. Carbon monoxide and nitrogen have similar ground-state electronic structures, comparable rotational constants,[29] nearly the same molecular mass, and similar triple points and critical points.[30] Figure 2 compares our new sound

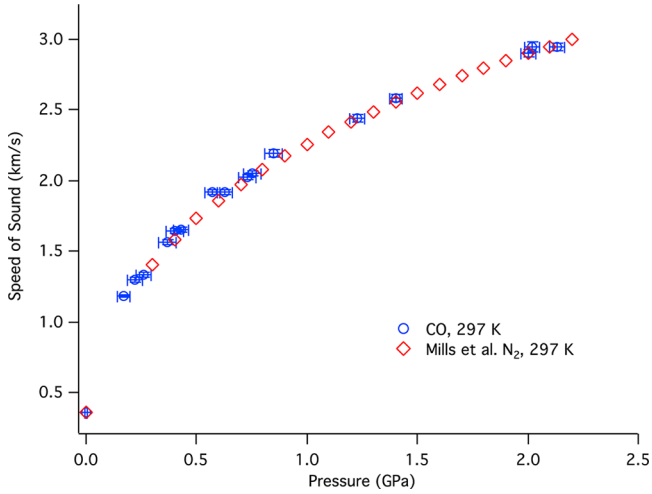

Figure 2. Sound speed comparison between CO (blue circles) and N_2 (red diamonds) along the 297 K isotherm. The N_2 data was obtained from Mills et al.,[31] and the CO datum nearest 0 GPa was obtained from ref 13.

speed measurements for CO to previously published[31] sound speeds for N_2. Within the experimental uncertainty, the data sets are identical, indicating that the repulsive components of the intermolecular potentials are also quite similar for these two molecular fluids.

Predicting the properties of simple molecular fluids such as CO at high pressures and temperatures is important for problems ranging from geophysics[32] to shock physics and detonation phenomena.[5] Ross and Ree have pointed out[33] that isotropic exponential-6 potentials are well suited for many such fluids particularly at strongly supercritical conditions, despite the fact that the molecules themselves can display fairly significant anisotropy. The fundamental basis of this approach, which replaces anisotropic interactions with effective spherical ones that enable fast and accurate thermodynamic calculations, is reasonably well understood[34,35] and some inverse applications have also been considered.[36,37] For molecules with significant dipole moment the original Ross variational theory[33] can be extended to account for the polar character of the intermolecular interactions and was successfully applied to water[38] and other molecular fluids and their mixtures.[5,22,39] One of the advantages of this approach, based on effective intermolecular potentials, is that the thermodynamics is minimally parametrized and thus can be well constrained by experimental data, and perhaps extrapolated with some confidence in thermodynamic regimes where the data may be scarce or physically unobtainable.

We employed this method to determine suitable exponential-6 parameters for CO using the speed of sound data presented in this paper, as well as previously available experimental data under static and shock conditions.[11,14,15,40] We only used shock wave data below 10 GPa, since experiments and simulations

dx.doi.org/10.1021/jp401510m | J. Phys. Chem. B 2013, 117, 5675−5682

suggest that at higher shock pressure CO likely starts dissociating.[14] Carbon monoxide has a small dipole moment, which has a very limited effect on the equation of state at high pressures. We set its value to the one measured for the isolated molecule, although, under condensed conditions the appropriate dipole moment may be somewhat larger.[38] Such effects, however, should be negligible for the range of pressures and temperatures that we are interested in.

We derive CO exponential-6 parameters by matching theoretical predictions[38] to a range of experimental data. A figure of merit was determined by averaging differences between calculated and experimental properties, and an automatic fitting routine was used to determine optimal parameters. Shock Hugoniot P−V data from Nellis et al.[14] below 10 GPa was employed in the fitting procedure, as well as PVT Hugoniot measurements by Moore et al.[15] Static data was used to constrain the EOS across a wider range of thermodynamic states. The PVT measurements of Robertson and Babb[11] and sound speed measurements of Extrada-Alexanders[40] between 0.25 and 2 MPa were used to constrain the EOS at lower pressure. The PVT data of Michels[10] between 2 and 200 MPa were also employed in the calibration procedure. Finally, we used the sound speed data reported here at 300 K in determining the potential parameters.

The optimal parameters reproduce very well the static high pressure and shock Hugoniot results, while providing very reasonable agreement with the sound speed measurements. The EXP-6 parameters, r_0 = 4.19 Å, ε/k_B = 90.00 K, α = 13.27, and dipole moment of 0.12 D, provide the best agreement with experimental observables, and is referred to as LLNL EXP-6 though out this manuscript.

Figure 3A,B shows the comparison between the calculated sound speeds from several EOS models and the experimentally measured values under static compression for 297 and 600 K, respectively. Adiabatic sound speed calculations utilizing exp6-polar thermodynamics[5] were conducted with CHEETAH—a thermochemical code that implements such statistical mechanics-based fluid theories, and which is typically used to solve chemical equilibrium problems involving complex mixtures under detonation or planetary interior conditions.[5,38] Pressure-dependent speeds of sound were also calculated using CHEETAH for a previously published intermolecular potential for CO.[18] The sound speeds for the Lemmon and Span[16] and the Xiang and Deiters[20] models − both corresponding states models − were calculated analytically from the parametrized Helmholtz energy expressions.[16] The calculated sound speeds for the LLNL EXP-6 potential at 297 K underestimate the measurements with a maximum deviation of 9.7% at low pressures and minimum deviation of 2.5% at higher pressures. The models of Lemmon et al. and Xiang et al. are parametrized using data in the MPa pressure range, and thus reproduce low-pressure sound speeds quite well, while at 1 GPa the respective 297 K velocities are 13.1% and 14.9% below PALS measurements. The Lemmon et al. and Xiang et al. CO sound speeds deviate from PALS data monotonically with pressure. The intermolecular potential, parametrized by Belonoshko et al., predicts sound speeds to within 1.8% at elevated pressures and to within 7.2% at the lower pressures. Other EOS models have been published for CO; however, one generally has no way of quickly calculating pressure-dependent sound speeds for comparison. Boshkova and Deiters[41] developed a soft-core repulsion correction—including quantum effect corrections—to the Kim et al.[42] simplified perturbed-hard-chain-theory

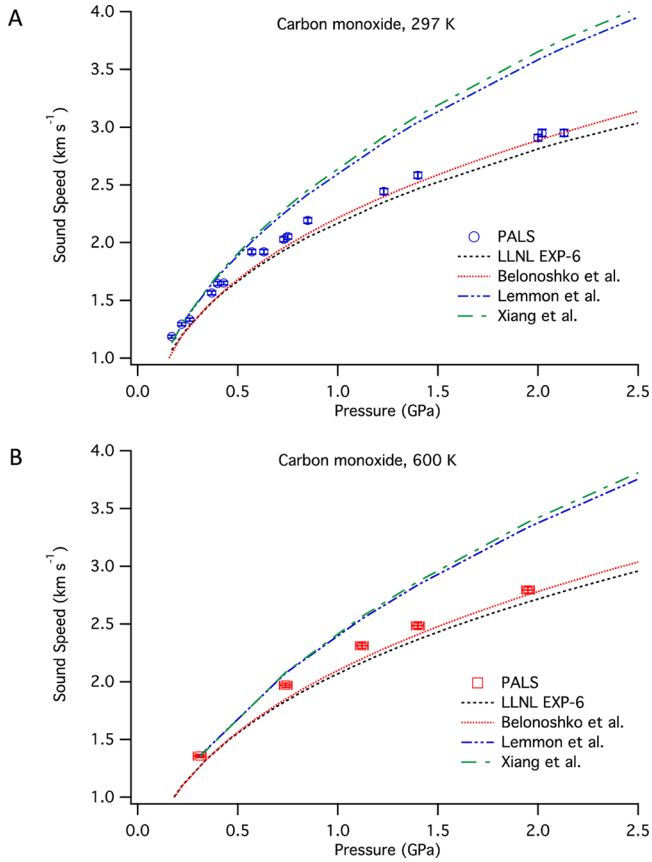

Figure 3. (A,B) Comparison of experimental sound speed data with calculated sound speeds from various EOS models for 297 and 600 K, respectively. The PALS data points are those reported in this manuscript. The LLNL EXP-6 curve (black dashed line) is calculated using CHEETAH with the EXP-6 potential reported in this manuscript. The curve labeled Belonoshko et al. (red dotted line) was generated by CHEETAH using the EXP-6 potential previously reported in ref 18. The Lemmon et al. (blue dash-dotted line) and Xiang et al. (green dash-dotted line) curves were calculated analytically using the EOSs provided in refs 16 and 20, respectively.

(sSPHCT) EoS model where predictions are derived from critical data only. An available sSPHCT online calculator tool provided by the Deiters group at the University of Cologne was utilized to compare CO speeds of sound values to PALS data. At 297 K and at 0.17 and 2.00 GPa respectively, the sSPHCT model sound velocities are 16.4% and 10.9% above the measured values.

Calculated Hugoniot points starting from initial densities consistent with the experimental shock experiments[14,15] are compared to the experimental data in Figure 4. The calculations were conducted with CHEETAH using both the new intermolecular potential and the potential of Belonoshko et al.[18] For shock compression, the LLNL EXP-6 potential reproduced the experimental densities to within <4% at low pressures, and to within <2% at higher pressures. The potential of Belonoshko et al. underestimates the density consistently by 4−5%. For comparison, the experimental error of the shocked fluid density is ∼2% for the work of Moore et al.[15] and ∼1% for that of Nellis et al.[14] The performance of the Belonoshko et al. potential at these high pressures and temperatures is quite impressive, considering this potential was parametrized with data extending to 1 GPa.[18]

dx.doi.org/10.1021/jp401510m | J. Phys. Chem. B 2013, 117, 5675−5682

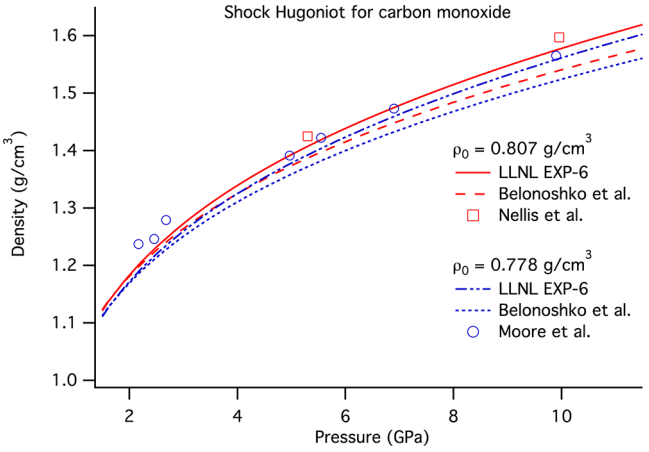

Figure 4. Shock Hugoniot comparison between the experimental data of Nellis et al.[14] and Moore et al.,[15] and CHEETAH-calculated Hugoniot states using both the LLNL EXP-6 and Belonoshko et al.[18] intermolecular potentials. Calculations starting with an initial density of 0.807 g/cm^3 for the LLNL EXP-6 potential (red line) and the Belonoshko et al. potential (red dashed line) are compared to the Nellis et al. experimental points (red squares). The other calculations starting with an initial density of 0.778 g/cm^3 for the LLNL EXP-6 potential (blue dotted-dashed line) and the Belonoshko et al. potential (blue dotted line) are compared to the Moore et al. experimental points (blue circles).

Figure 5 shows the PρT surface calculated with CHEETAH for the CO fluid phase up to 2000 K and 10 GPa. Above those

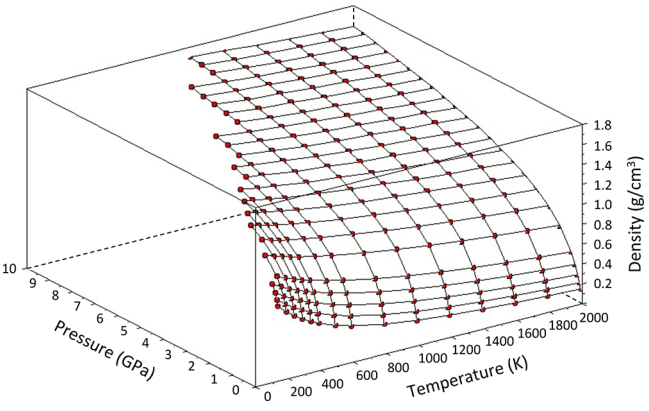

Figure 5. Grid of PρT points calculated with CHEETAH using the LLNL EXP-6 intermolecular potential.

PT extremes molecular CO has an abrupt increase in absorption and is thought to undergo dissociation.[15] At pressures below 1 GPa, the calculated densities along the 300 K isotherm are within 0.8% of the experimentally measured values.[11] On the basis of previous experience with these types of calculations, we expect a similar deviation for other PρT points.

These PρT states were subsequently fit to a polynomial EOS,[43]

$$\rho = A + BP^{(-1)} + C\sqrt{P} + DP + EP^2 + EF^3 \quad (1)$$

where the density ρ (g/cm^3) is a function of the hydrostatic pressure P (GPa), and A, B, C, D, E, and F are temperature-dependent coefficients. The explicit temperature dependence of each coefficient was determined empirically and is given in eq 2. The temperature is in Kelvin.

$$A = A_0 + A_1 e^{-A_2 T} \quad (2a)$$

$$B = B_0 + B_1 T^{-1} + B_2 T + B_3 T^{-2} + B_4 T^2 \quad (2b)$$

$$C = C_0 + C_1 T^{-1} + C_3 T^{-2} \quad (2c)$$

$$D = D_0 + D_1 e^{-D_2 T} \quad (2d)$$

$$E = E_0 + E_1 T^{-1} + E_3 T^{-2} \quad (2e)$$

$$F = F_0 + F_1 e^{(-F_2 T)} \quad (2f)$$

The entire surface was optimized simultaneously using multivariate least-squares regression of eqs 1 and eq 2. The fitting results are compiled in Table 2 and reproduce the

Table 2. EOS Parameters for Carbon Monoxide Obtained through Multivariate Least Squares Regression[a]

	i = 0	1	2	3	4
A_i	−3.6139 × 10^{-1}	8.7538 × 10^{-1}	1.0025 × 10^{-3}		
B_i	−4.5447 × 10^{-2}	1.1328 × 10^{1}	3.6798 × 10^{-5}	−7.3938 × 10^{2}	−7.4528 × 10^{-9}
C_i	1.2020 × 10^{0}	−2.1440 × 10^{1}	2.5993 × 10^{3}		
D_i	−2.9305 × 10^{-1}	−2.8965 × 10^{-1}	2.8744 × 10^{-3}		
E_i	1.6612 × 10^{-2}	−4.0062 × 10^{0}	3.9915 × 10^{3}		
F_i	−5.6078 × 10^{-}	−3.6802 × 10^{0}	2.4101 × 10^{-2}		

[a]These constants have units such that the densities are calculated in g/cm^3, as long as the pressure and temperature are provided in units of GPa and K.

CHEETAH values with a root-mean-squared deviation of 0.45%, and a maximum deviation of 1.2%. The percent differences are well described by a Gaussian distribution having a standard deviation of 0.48%, and 98% of CHEETAH-calculated PρT states are reproduced with an error less than 1% using the above analytical EOS. Accordingly, the analytic EOS parametrized here should be good to within <2.5% of the actual experimental densities, if measurements were feasible.

This CO EOS is optimized for a wide range of pressure (0.1 to 10 GPa) and temperature conditions (150 to 2000 K), and is expected to have higher accuracy at pressures above 0.5 GPa. The polynomial form was chosen to yield an optimal fit with the exp6-polar EoS[5] over this range of thermodynamic conditions, and it should not be used to make predictions below 0.1 GPa or above 10 GPa; outside this range we recommend using directly the exp6-polar EoS, with the parameters quoted in the manuscript. We note that an initial attempt was made to parametrize the Tait EoS since the equation includes the material compressibility. Unfortunately the Tait EoS was unable to satisfactorily reproduce the curvature of higher density data. Figure 6 compares the experimental measurements of Robertson et al.[11] with the CHEETAH calculated PρT states using the LLNL EXP-6 parameters and with the EOS parametrized above. The deviation between the experimentally determined densities and the EOS model is reported as percent error. While the LLNL EXP-6 calculations are within <1% of the experimental

dx.doi.org/10.1021/jp401510m | J. Phys. Chem. B 2013, 117, 5675−5682

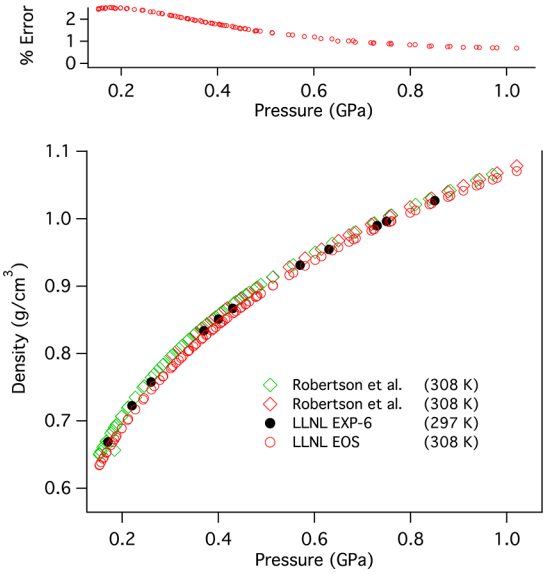

Figure 6. Comparison of experimental densities,[11] calculated densities using LLNL EXP-6, and calculated densities using the analytical EOS of eq 1. The percent error is calculated between the experimental data of Robertson et al. and the LLNL EOS calculated values. Both data sets are labeled "308 K" within the legend. However, the green diamonds correspond to 307.96 K, while the red diamonds correspond to 308.00 K.

values, the parametrized EOS exhibits an increased error at low pressures. Introducing additional EOS fit parameters would certain help our ability to reproduce the low-pressure data; however, existing EOS models[16,20] were optimized for these lower pressures.

Given the success in modeling the CO fluid state using the spherical molecular interactions-based framework, we decided to inquire to what extent such interactions could be transferred to the solid state. Kang and Ree[44] have developed and tested a solid-state variational theory for exponential-6 fluids, which performs very well for predicting the fluid- and solid-state thermodynamic properties, including the melting line, of rare gases such as argon. Carbon monoxide is, however, an anisotropic molecule, and it is not clear if orientational averaging, due to either rotational motion or disorder, can result in the same effective spherical potential in the solid phase with the one that is appropriate for the fluid phase. To test this hypothesis, we performed calculations using the Kang and Ree[44] solid variational theory (without including polar contributions) for the CO β phase, and compared with available experimental results. The β phase was assumed to exhibit disordered molecules with no net polarization, as suggested by Cromer et al.[45]

These calculated densities for the β-phase, along with the experimental ones,[46] are displayed in Table 3. The agreement between theory and experiment for the density is on average ~2%, which, although not as good as for the fluid, is nonetheless fairly remarkable. The reported experimental errors in the pressure and volume measurements are similar in magnitude.[46] This indicates that it may be possible to have a reasonably accurate unified thermodynamic treatment based on spherical interactions even for some small anisotropic molecules. Such an approach may be useful, for example, to design experiments, e.g., shock wave experiments, which cross the fluid−solid phase line.

Table 3. Comparison of Calculated Volumes for the β-Phase of CO and Experimental Volumes for Several Pressures at 300 K

pressure[a] (GPa)	temperature (K)	calculated volume (cm^3/mol)	exp. volume[b] (cm^3/mol)	% difference[c]
3.8 ± 0.1	300	18.78	19.47[d]	3.5
3.9 ± 0.0	300	18.68	18.94 ± 0.30	1.4
4.1 ± 0.1	300	18.49	18.95 ± 0.13	2.4
4.1 ± 0.2	300	18.49	18.77[d]	1.0
4.1 ± 0.1	300	18.49	19.04 ± 0.08	2.9
4.3 ± 0.1	300	18.30	18.82 ± 0.03	2.8
4.4 ± 0.0	300	18.22	18.31 ± 0.20	0.5
5.2 ± 0.0	300	17.58	17.93[d]	2.0

[a]Pressures with error reported in Table 5 from ref 46. [b]Experimental molar volumes from ref 46. [c]The percent difference is calculated between the calculated and experimental molar volumes. [d]Error in molar volume not reported in ref 46.

Pressing further to test the possibility of a unified thermodynamic treatment, we initially set out to calculate the melt line between the fluid and β-solid phases with the new potential and compare this to the experimentally determined boundary. This effort was thwarted by surprisingly few experimental measurements of the melt line, along with an unknown degree of rotational freedom of CO molecules in the β phase.[45,47,48] Instead, we decided to calculate these phase boundaries assuming two extremes: no rotational freedom and full rotational freedom. Figure 7 displays the phase boundaries corresponding to the two physical extremes plotted along with the other known phase boundaries for CO.[49]

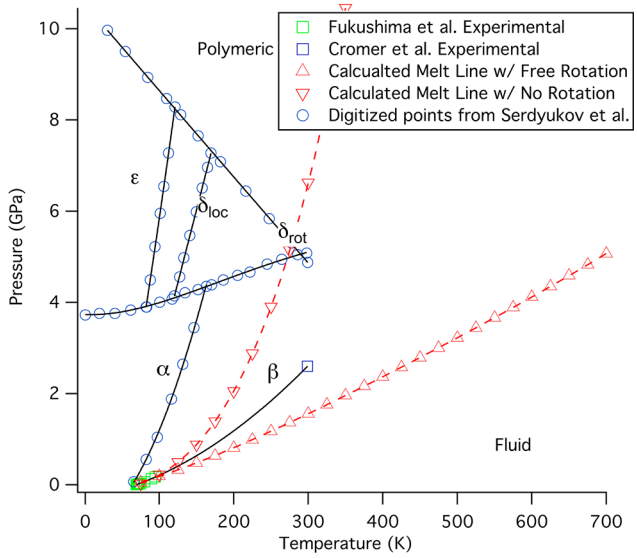

Figure 7. Phase diagram of carbon monoxide. Low-pressure features such as the fluid-gas coexistence below the critical pressure of 3 MPa are not shown. The calculated phase boundary between the fluid phase and β-solid phase is shown assuming the two extremes: full rotation (upward, red triangles) and no rotation (downward, red triangles). The experimental boundary between the fluid phase and β-solid phase is generated from Fukushima et al.[47] (green squares) and Cromer et al.[45] (blue square). The phase line is a polynomial interpolation between those data sets. The other phase boundaries (blue circles) are digitized points from the recently published phase diagram of Serdyukov et al.[49]

dx.doi.org/10.1021/jp401510m | J. Phys. Chem. B 2013, 117, 5675−5682

We find that the calculated melt lines bound the experimental points of Fukushima et al.[47,48] and Cromer et al.[45] The experimental points are nearly centered between the calculation extremes at low temperatures. While not surprisingly, the room temperature point is positioned closer to the free-rotation model, yet likely still exhibits hindered rotation.

IV. SUMMARY

We have presented sound speed measurements for fluid CO up to hydrostatic pressures of several GPa along the 297 and 600 K isotherms. The CO 297 K isotherm sound speed data was then compared to the previously published sound speeds for N_2, revealing an identical pressure dependent behavior. We have also used this data to further refine an effective dipolar exponential-6 intermolecular potential. We calculated sound speeds and shock Hugoniots using the newly parametrized potential and compared them to both experimental results and other EOS models. These comparisons show that the new potential is broadly applicable to both static and dynamic compression experiments. The LLNL EXP-6 potential was incorporated in to the CHEETAH thermochemical code and subsequently used to calculate PρT states for CO, extending to pressures and temperatures associated with shock-induced molecular dissociation. An analytical EOS model for CO was also fit to the calculated PρT states, and is presented for those without access to either CHEETAH or an alternative thermochemical code.

AUTHOR INFORMATION

Corresponding Author

*E-mail: zaug1@llnl.gov.

Notes

The authors declare no competing financial interest.

ACKNOWLEDGMENTS

We thank Prof. Evan Abramson for providing our group with Sm:SrB_4O_7 single crystals. We also acknowledge Prof. Mike Brown for providing us with his IAPWS MatLab code used to calculate the sound velocity of pressurized fluid water. This research was partly funded by the Joint DoD/DOE Munitions Program, and was performed under the auspices of the U.S. Department of Energy by Lawrence Livermore National Laboratory under Contract No. DE-AC52-07NA27344.

REFERENCES

(1) Huizenga, J. Thermodynamic Modelling of C−O−H Fluids. *Lithos* **2001**, *55*, 101−114.
(2) Huizenga, J. Thermodynamic Modelling of a Cooling C−O−H Fluid Graphite System: Implications for Hydrothermal Graphite Precipitation. *Miner. Deposita* **2011**, *46*, 23−33.
(3) Boulard, E.; Gloter, A.; Corgne, A.; Antonangeli, D.; Auzende, A.; Perrillat, J.; Guyot, F.; Fiquet, G. New Host for Carbon in the Deep Earth. *Proc. Natl. Acad. Sci. U.S.A.* **2011**, *108*, 5184−5187.
(4) Jakobsson, S.; Oskarsson, N. The System C−O in Equilibrium with Graphite at High-Pressure and Temperature - An Experimental-Study. *Geochim. Cosmochim. Acta* **1994**, *58*, 9−17.
(5) Bastea, S.; Fried, L. E. Chemical Equilibrium Detonation. In *Shock Wave Science and Technology Reference Library*; Springer-Verlag: Berlin Heidelberg, 2012; Vol. *6*; pp 1−31.
(6) Riazi, M.; Mansoori, G. Use of the Velocity of Sound in Predicting the PVT Relations. *Fluid Phase Equilib.* **1993**, *90*, 251−264.
(7) Goodwin, R. Carbon-Monoxide Compressibility Data from 100 to 300 K; Derived Virial Coefficients, Orthobaric Densities, and Heats of Vaporization. *Cryogenics* **1983**, *23*, 403−414.
(8) Goodwin, R. Carbon Monoxide Thermophysical Properties from 68 to 1000 K at Pressures to 100 MPa. *J. Phys. Chem. Ref. Data* **1985**, *14*, 849−933.
(9) Bartlett, E.; Hetherington, H.; Kvalnes, H.; Tremearne, T. The Compressibility Isotherms of Carbon Monoxide at Temperatures from −70 to 200 Degrees and at Pressures to 1000 atm. *J. Am. Chem. Soc.* **1930**, *52*, 1374−1382.
(10) Michels, A.; Lupton, J.; Wassenaar, T.; Degraff, W. Isotherms of Carbon Monoxide between 0°C and 150°C and at Pressures Up to 3000 atm. *Physica* **1952**, *18*, 121−127.
(11) Robertson, S.; Babb, S. Isotherms of Carbon Monoxide to 10 kbar and 300°C. *J. Chem. Phys.* **1970**, *53*, 1094−1097.
(12) Hilsenrath, J.; Beckett, C. W.; Benedict, W. S.; Fano, L.; Hoge, H. J.; Masi, J. F.; Nuttall, R. L.; Touloukian, Y. S.; Woolley, H. W. Tables of Thermal Properties of Gases. In *Circulars of the National Bureau of Standards*; U.S. Printing Office: Washington, DC, 1957; Issue 564, p 486.
(13) Van Itterbeek, A.; Mariens, P. Measurements with Ultrasonics on the Velocity and Absorption of Sound at Ordinary and at Low Temperatures. *Physica* **1937**, *4*, 609−616.
(14) Nellis, W.; Ree, F.; Vanthiel, M.; Mitchell, A. Shock Compression of Liquid Carbon Monoxide and Methane to 90 GPa (900 kbar). *J. Chem. Phys.* **1981**, *75*, 3055−3063.
(15) Moore, D.; Schmidt, S.; Shaw, M.; Johnson, J. Coherent Anti-Stokes Raman Spectroscopy of Shock-Compressed Liquid Carbon Monoxide. *J. Chem. Phys.* **1991**, *95*, 5603−5608.
(16) Lemmon, E.; Span, R. Short Fundamental Equations of State for 20 Industrial Fluids. *J. Chem. Eng. Data* **2006**, *51*, 785−850.
(17) Baniasadi, M.; Ghader, S. New Isotherm Regularity and an Equation of State for Gases and Liquids. *J. Ind. Eng. Chem.* **2012**, *18*, 474.
(18) Belonoshko, A.; Saxena, S. A Molecular-Dynamics Study of the Pressure−Volume−Temperature Properties of Supercritical Fluids: II. CO_2, CH_4, CO, O_2, and H_2. *Geochim. Cosmochim. Acta* **1991**, *55*, 3191−3208.
(19) Saeki, S. Empirical Equation of State for Supercritical Fluids. *J. Supercrit. Fluids* **1995**, *8*, 30−45.
(20) Xiang, H.; Deiters, U. A New Generalized Corresponding States Equation of State for the Extension of the Lee-Kesler Equation to Fluids Consisting of Polar and Larger Nonpolar Molecules. *Chem. Eng. Sci.* **2008**, *63*, 1490−1496.
(21) Buckingham, R. The Classical Equation of State of Gaseous Helium, Neon and Argon. *Proc. R. Soc. London, Ser. A* **1938**, *168*, 264−283.
(22) Zaug, J.; Bastea, S.; Crowhurst, J.; Armstrong, M.; Teslich, N. Photoacoustically Measured Speeds of Sound of Liquid HBO_2: Semi-Empirical Modeling of Boron Containing Explosives. *J. Phys. Chem. Lett.* **2010**, *1*, 2982−2988.
(23) Lipp, M.; Evans, W.; Garcia-Baonza, V.; Lorenzana, H. Carbon Monoxide: Spectroscopic Characterization of the High-Pressure Polymerized Phase. *J. Low Temp. Phys.* **1998**, *111*, 247−256.
(24) Abramson, E.; Brown, J. Equation of State of Water Based on Speeds of Sound Measured in the Diamond-Anvil Cell. *Geochim. Cosmochim. Acta* **2004**, *68*, 1827−1835.
(25) Abramson, E.; Brown, J.; Slutsky, L.; Wiryana, S. Measuring Speed of Sound and Thermal Diffusivity in the Diamond-Anvil Cell. *Int. J. Thermophys.* **2001**, *22*, 405−414.
(26) Jansen, L.; Michels, A.; Lupton, J. Contribution to the Analysis of Molecular Interactions in Compressed Nitrogen and Carbon Monoxide: I. The Molecular Field in the High Density Gas State. *Physica* **1954**, *20*, 1215−1234.
(27) Jansen, L.; Michels, A.; Lupton, J. Contribution to the Analysis of Molecular Interactions in Compressed Nitrogen and Carbon Monoxide: II. Quadrupole Moments and Properties of the Solid States. *Physica* **1954**, *20*, 1235−1243.
(28) Jansen, L.; Michels, A.; Lupton, J. Contribution to the Analysis of Molecular Interactions in Compressed Nitrogen and Carbon Monoxide: III. Quadrupole Orientation and Induction Effects at High Temperatures. *Physica* **1954**, *20*, 1244−1249.

(29) Huber, K. P.; Herzberg, G. Constants of Diatomic Molecules. In *NIST Chemistry WebBook*, NIST Standard Reference Database Number 69; Linstrom, P. J., Mallard, W. M., Eds.; National Institutes of Standards and Technology: Gaithersburg, MD, 2003 (http://webbook.nist.gov).
(30) Burgess, D. R. Thermochemical Data. In *NIST Chemistry WebBook*, NIST Standard Reference Database Number 69; Linstrom, P. J., Mallard, W. M., Eds.; National Institutes of Standards and Technology: Gaithersburg, MD, 2003 (http://webbook.nist.gov).
(31) Mills, R.; Liebenberg, D.; Bronson, J. Sound Velocity and Equation of State of N_2 to 22 kbar. *J. Chem. Phys.* **1975**, *63*, 1198−1204.
(32) Churakov, S.; Gottschalk, M. Perturbation Theory Based Equation of State for Polar Molecular Fluids: I. Pure Fluids. *Geochim. Cosmochim. Acta* **2003**, *67*, 2397−2414.
(33) Ross, M.; Ree, F. Repulsive Forces of Simple Molecules and Mixtures at High Density and Temperature. *J. Chem. Phys.* **1980**, *73*, 6146−6152.
(34) Shaw, M.; Johnson, J.; Holian, B. Effective Spherical Potentials for Molecular Fluid Thermodynamics. *Phys. Rev. Lett.* **1983**, *50*, 1141−1144.
(35) Lebowitz, J.; Percus, J. One-Dimensional Models of Anisotropic Fluids. *Ann. N.Y. Acad. Sci.* **1983**, *410*, 351−359.
(36) Bastea, S.; Ree, F. Consistent Anisotropic Repulsions for Simple Molecules. *Phys. Rev. B* **2000**, *62*, 5478−5481.
(37) Belonoshko, A.; Rosengren, A.; Skorodumova, N.; Bastea, S.; Johansson, B. Shock Wave Propagation in Dissociating Low-Z Liquids: D_2. *J. Chem. Phys.* **2005**, *122*, 124503−1−8.
(38) Bastea, S.; Fried, L. Exp6 Polar Thermodynamics of Dense Supercritical Water. *J. Chem. Phys.* **2008**, *128*, 174502−1−4.
(39) Maiti, A.; Bastea, S.; Howard, W.; Fried, L. Nitrous Acid Under High Temperature and Pressure - From Atomistic Simulations to Equation of State for Thermochemical Modeling. *Chem. Phys. Lett.* **2009**, *468*, 197−200.
(40) Estrada-Alexanders, A.; Hurly, J. Kinematic Viscosity and Speed of Sound in Gaseous CO, CO_2, SiF_4, SF_6, C_4F_8, and NH_3 from 220 to 375 K and Pressures Up to 3.4 MPa. *J. Chem. Thermodyn.* **2008**, *40*, 193−202.
(41) Boshkova, O.; Deiters, U. Soft Repulsion and the Behavior of Equations of State at High Pressures. *Int. J. Thermophys.* **2010**, *31*, 227−252.
(42) Kim, C.-H.; Vimalchand, P.; Donohue, M.; Sandler, S. Local Composition Model for Chainlike Molecules: A Simplified Version of the Perturbed Hard Chain Theory. *AIChE J.* **1986**, *32*, 1726−1734.
(43) Franck, E.; Wiegand, G.; Gerhardt, R. The Density of Hydrogen Fluoride at High Pressures to 973 K and 200 MPa. *J. Supercrit. Fluids* **1999**, *15*, 127−133.
(44) Kang, H.; Ree, F. A Variational Theory of Classical Solids. *J. Chem. Phys.* **1993**, *99*, 2985−2991.
(45) Cromer, D.; Schiferl, D.; Lesar, R.; Mills, R. Room Temperature Structure of Carbon-Monoxide at 2.7 and 3.6 GPa. *Acta Crystallogr., Sect. C: Cryst. Struct. Commun.* **1983**, *39*, 1146−1150.
(46) Mills, R.; Olinger, B.; Cromer, D. Structures and Phase Diagrams of N_2 and CO to 13 GPa by X-ray-Diffraction. *J. Chem. Phys.* **1986**, *84*, 2837−2845.
(47) Fukushima, E.; Gibson, A.; Scott, T. Carbon-13 NMR of Carbon Monoxide. I. Pressure Dependence of Translational Motion in β-CO. *J. Chem. Phys.* **1977**, *66*, 4811−4817.
(48) Fukushima, E.; Gibson, A.; Scott, T. Pressure Dependence of Melting and $\alpha-\beta$ Phase Transition Temperatures of Carbon-Monoxide. *J. Low Temp. Phys.* **1977**, *28*, 157−165.
(49) Serdyukov, A.; Vetter, M.; Brodyanski, A.; Jodl, H. Lattice Phonons of Solid Phases (α,β,δ,ε) of Carbon Monoxide by Optical Studies. *Low Temp. Phys.* **2010**, *36*, 424−438.